Published in final edited form as:

Curr Biol. 2022 November 21; 32(22): 4957–4966.e5. doi:10.1016/j.cub.2022.09.048.

Sleep Need-Dependent Changes in Functional Connectivity Facilitate Transmission of Homeostatic Sleep Drive

Margaret C.W. Ho[*,1], **Masashi Tabuchi**[*,2], **Xiaojun Xie**[3], **Matthew Brown**[4], **Skylar Luu**[1], **Serena Wang**[1], **Alex Kolodkin**[4], **Sha Liu**[5], **Mark N. Wu**[1,4,#,^]

[1]Department of Neurology, Johns Hopkins University School of Medicine, Baltimore MD 21205, U.S.A.

[2]Department of Neurosciences, Case Western Reserve University, Cleveland, OH 44106, U.S.A.

[3]The Children's Hospital, Zhejiang University School of Medicine, National Clinical Research Center for Child Health, Hangzhou, Zhejiang, China

[4]Department of Neuroscience, Johns Hopkins University School of Medicine, Baltimore MD 21205, U.S.A.

[5]VIB Center for Brain & Disease Research and Department of Neurosciences, KU Leuven, Leuven 3000, Belgium.

Summary

How the homeostatic drive for sleep accumulates over time and is released remains poorly understood. In *Drosophila*, we previously identified the R5 ellipsoid body (EB) neurons as putative sleep drive neurons[1] and recently described a mechanism by which astrocytes signal to these cells to convey sleep need[2]. Here, we examine the mechanisms acting downstream of the R5 neurons to promote sleep. EM connectome data demonstrate that R5 neurons project to EPG neurons[3]. Broad thermogenetic activation of EPG neurons promotes sleep, while inhibiting these cells reduces homeostatic sleep rebound. Perforated patch-clamp recordings reveal that EPG neurons exhibit elevated spontaneous firing following sleep deprivation, which likely depends on an increase in extrinsic excitatory inputs. Our data suggest that cholinergic R5 neurons participate in the homeostatic regulation of sleep, and epistasis experiments indicate that the R5 neurons act upstream of EPG neurons to promote sleep. Finally, we show that the physical and functional connectivity between the R5 and EPG neurons increases with greater sleep need. Importantly, dual patch-clamp recordings demonstrate that activating R5 neurons induces cholinergic-dependent excitatory post-synaptic responses in EPG neurons. Moreover, sleep loss triggers an increase in the amplitude of these responses, as well as in the proportion of EPG neurons that respond. Together,

[#]Correspondence: marknwu@jhmi.edu.
[*]These authors contributed equally to this work
[^]Lead contact

Author Contributions

Conceptualization, MCWH, MT, MNW; Methodology, MCWH, MT, SL, MB; Investigation, MCWH, MT, SL, XX, MB, SL, SW; Writing – Original Draft, MCWH, MT, MNW; Writing – Review & Editing, MCWH, MT, SL, XX, MB, SL, SW, AK, MNW; Resources, AK, MNW; Visualization, MCWH, MT, SL, XX; Supervision, MCWH, AK, MNW; Funding Acquisition, MCWH, MT, AK, SL, MNW.

Declaration of Interests

The authors declare no competing interests.

our data support a model whereby sleep drive strengthens the functional connectivity between R5 and EPG neurons, triggering sleep when a sufficient number of EPG neurons are activated. This process could enable the proper timing of the accumulation and release of sleep drive.

eTOC Blurb

The circuit mechanisms underlying the homeostatic regulation of sleep remain enigmatic. Ho et al. find that sleep deprivation induces plastic changes in a homeostatic sleep circuit, which potentiates signaling to a downstream sleep-promoting circuit. They propose that this process mediates transmission of homeostatic sleep drive in *Drosophila*.

Results and Discussion

EPG neurons promote sleep and contribute to sleep homeostasis

We recently delineated a pathway signaling sleep need from astrocytes to the ellipsoid body (EB) R5 sleep drive neurons in *Drosophila*[2]. To further elucidate the circuit mechanisms underlying the homeostatic regulation of sleep, we sought to identify neuronal groups that act downstream of the R5 neurons in this process. The fly hemibrain connectome data demonstrate that R5 neurons synapse with EPG ("compass") neurons, shown to be involved in navigation[3–6]. As expected, a split-GAL4 driver for R5 neurons (*R30G03-AD, R58H05-DBD*) driving expression of DenMark[7] and synaptotagmin-GFP[8] (syt-GFP) labelled synaptic terminals in the EB ring, while *R19G02-GAL4>UAS-DenMark, UAS-syt-GFP* flies (labelling EPG neurons) demonstrated both synaptic terminal and dendritic labeling throughout the EB ring and additional synaptic terminal staining in the protocerebral bridge (PB) (Figures S1A and S1B). Intriguingly, we previously performed a large-scale screen for GAL4 lines affecting sleep behavior, and *R19G02-GAL4* (Figures 1A and S1C) was identified as a driver inducing increased sleep during neural activation with dTRPA1[1]. We repeated those findings and obtained similar results with thermogenetic activation of an additional split-GAL4 line (*SS50574*) that also drives restricted expression in EPG neurons (Figures 1B, 1C, S1D, and S1E). The sleep induced by heat treatment of *R19G02-GAL4>UAS-dTRPA1* or *SS50574>UAS-dTRPA1* flies was more consolidated with longer sleep bout duration and reduced sleep bout number, compared to controls (Table S1).

To address whether the quiescent behavior seen with activation of these drivers simply represented locomotor inactivity, we performed arousal threshold experiments. As shown in Figures 1D and 1E, flies during these consolidated quiescent states displayed a significant increase in arousal threshold to submaximal mechanical stimulation, compared to awake flies. Because EPG neurons function in navigation, we next asked whether thermogenetic activation of EPG neurons caused locomotor impairment. First, *R19G02-GAL4>UAS-dTRPA1* or *SS50574>UAS-dTRPA1* flies were subjected to 2 hr heat treatment at 29°C, and climbing ability was assessed. Climbing ability was similar for these genotypes compared to controls (Figure S1F). Second, we analyzed peak activity data following strong mechanical stimuli from our arousal threshold experiments at 29°C. The peak activity of *SS50574>UAS-dTRPA1* flies was similar to controls, while it was reduced for *R19G02-GAL4>UAS-dTRPA1* flies (Figure S1G). Together, these data argue that activation

of EPG neurons promotes sleep and not behavioral quiescence due to locomotor inactivity or impairment.

To further confirm that the increased sleep phenotype maps to EPG neurons, we tested additional GAL4 drivers that label these cells (*R15C03-GAL4* and *R60D05-GAL4*)[5,9,10]. Unexpectedly, thermogenetic activation using these drivers did not enhance sleep (Figure S1I). We hypothesized that these phenotypic differences could arise from 1) differences in driver strength, 2) a requirement for a distinct subset, or 3) a need for a sufficient number of EPG cells. To address issues related to driver strength, we repeated these experiments using a stronger effector (*20XUAS-dTRPA1*). However, under these conditions, sleep was still not induced using the *R60D05-GAL4* and *R15C03-GAL4* drivers (Table S1). Interestingly, examination of Multi-Color Flp Out (MCFO)[11] data from the HHMI Janelia imaging database[12] suggests relatively limited expression in EPG neurons for the *R15C03-GAL4* driver, compared to *R19G02-GAL4* (*R60D05-GAL4* was not included in this MCFO analysis). Thus, we next combined the *R60D05-GAL4* + *R15C03-GAL4* drivers to perform thermogenetic activation, which resulted in increased sleep amount (Figures S1H and S1I and Table S1). To examine the relationship between EPG cell number and the ability of a given driver to promote sleep, we performed cell counting analyses. The two EPG driver lines that do not promote sleep (*R15C03-GAL4* and *R60D05-GAL4*) label the fewest presumed EPG neurons, whereas *R19G02-GAL4*, *SS50574*, and *R15C03-GAL4*+*R60D05-GAL4* label higher numbers of these cells (Figure S1J). These data suggest that activation of a sufficient number of EPG neurons is required to promote sleep.

We next asked whether EPG neurons are required for baseline sleep or homeostatic regulation of sleep. To address this question, we expressed tetanus toxin in EPG neurons (*R19G02-GAL4>UAS-TNT*) and measured sleep under baseline conditions and following mechanical sleep deprivation (SD). Inhibiting synaptic transmission of EPG neurons did not affect baseline daily sleep amount or consolidation (Table S1), but significantly reduced “rebound sleep” after 12 hr SD (Figures 1F and 1G). Together, these findings suggest that the EPG neurons are sleep-promoting and contribute to the homeostatic regulation of sleep.

Sleep need increases EPG neuron activity via extrinsic inputs

We next investigated whether EPG neuron activity is altered with increased sleep need. We performed perforated patch-clamp recordings of EPG neurons following either 12 hr of mechanical SD or undisturbed sleep (control) (Figure 2A). These experiments revealed a ~2-fold increase in spontaneous firing rate of EPG neurons in SD vs control animals (Figures 2B and 2C). This increase in spontaneous spiking of EPG neurons following SD was also reflected by a reduced interspike interval and an increase in instantaneous action potential (AP) firing rate (Figures S2A and S2B). These data suggest that sleep loss induces an increase in EPG neuron activity.

We conducted additional analyses to address whether this increase in EPG activity following SD was due to changes in extrinsic inputs or intrinsic excitability. There was no change in resting membrane potential (RMP) or AP threshold in EPG neurons following SD (Figures S2C and S2D). In addition, measurement of evoked spiking frequency following current injection did not reveal a significant increase in overall intrinsic excitability of

EPG neurons after sleep loss, compared to controls (although EPG spiking frequency was greater specifically with 100 pA current injections) (Figure S2E). These findings suggest that changes in extrinsic input, rather than intrinsic excitability, drive the increase in spontaneous firing of EPG neurons following sleep loss. To further address this possibility, we examined spontaneous excitatory post-synaptic potentials (EPSPs) in EPG neurons. As shown in Figures 2D and 2E, spontaneous EPSP frequency was greater in these cells after SD, compared to controls, suggesting an increase in excitatory synaptic inputs under these conditions. To assess for possible synaptic potentiation following SD, we examined EPSP amplitude and EPSP-spike coupling[13]. There was a significant increase in EPSP amplitude in EPG neurons under conditions of greater sleep need (Figures 2F and S2F). In addition, we observed a reduction in EPSP-spike latency in EPG cells following SD (Figures 2G and S2G), suggesting greater EPSP-spike coupling[14]. Together, these findings suggest that EPG neuron activity is increased with greater homeostatic sleep need, which is largely mediated by an increase in excitatory synaptic inputs onto these cells.

R5 neurons act upstream of EPG neurons to promote sleep

What is the presynaptic source of SD-triggered excitatory input to the EPG neurons? We hypothesized that the R5 neurons activate EPG neurons to signal sleep drive and induce sleep. However, the predominant mode of signaling within the EB ring is thought to be inhibitory (i.e., GABAergic)[15,16]. Thus, we first characterized the neurotransmitter identity of R5 neurons by performing immunostaining using antibodies against GABA, ChAT, and VGlut (Figure 3A). As expected, GABA neurotransmitter expression was observed throughout the ellipsoid body ring. Regarding R5 neurons specifically, colocalization of both anti-GABA and anti-ChAT signal with GFP signal was observed in R5 neuron axons (*R30G03-AD,R58H05-DBD>UAS-CD8::GFP*). In contrast, no vGluT signal was detected in the EB ring (Figure 3A). Next, to quantify the proportion of R5 neurons expressing different neurotransmitters, we performed double labeling experiments using *R58H05-QF2>QUAS-tdTomato* with anti-GABA antibody or *ChAT-* and *VGluT-GAL4* MIMIC lines[17] driving expression of Stinger-GFP. These analyses suggested that ~30% of R5 neurons are $GABA^+$ (6.8 out of 22.8 per brain) and that ~30% of R5 neurons are $ChAT^+$ (6.4 out of 20.4 neurons per brain). No overlap of R5 neurons was seen with neurons labeled by the VGluT MIMIC line (Figures 3B and 3C). Because we suspected that excitatory signals from R5 neurons act on EPG neurons to promote the homeostatic regulation of sleep, we performed ChAT knockdown in R5 neurons and assessed sleep before and after SD. We first confirmed that the *UAS-ChAT-miR* line could be used to knockdown ChAT expression (8411 ± 1266 arbitrary units (A.U.) for *MB247-GAL4>+* (n=6), 8413 ± 770 A.U. for *+>UAS-ChAT-miR* (n=6), and 2212 ± 682 A.U. for *MB247-GAL4>UAS-ChAT-miR* (n=6) flies, $P<0.001$, one-way ANOVA with post-hoc Tukey's test) (Figure S3A). Compared to controls, *R58H05-GAL4>UAS-ChAT-miR* flies exhibited a subtle reduction in rebound sleep after SD, but no change in baseline daily sleep (Figures 3D–3F).

We previously demonstrated that activation of R5 neurons promotes sleep both during and after the activation[1,2]. Recent work has found that some GAL4 drivers labeling R5 neurons also express in peripheral pickpocket-expressing (ppk) neurons[18]. Ppk^+ nociceptive neurons are found in the periphery on legs and in the fly abdominal body wall and have

been shown to promote arousal and subsequent "rebound" sleep[19,20]. We confirmed that *R30G03-GAL4* exhibits expression in peripheral neurons in the legs and abdominal body wall, while *R69F08-GAL4* and *R46C03-GAL4* labels peripheral neurons in the abdominal body wall (Figure S3B). In contrast, *R58H05-GAL4* did not drive detectable expression in peripheral neurons in the legs or abdomen, as was also the case for 2 split-GAL4 drivers (*R58H05-AD, R46C03-DBD* and *R30G03-AD, R58H05-DBD*) (Figure S3C and S3D). Thermogenetic activation of these drivers, as well as *R58H05-GAL4* combined with 2 copies of *ppk-GAL80*, recapitulated the increase in sleep during and after heat treatment (Figures S3E–S3J).

To investigate a role for EPG neurons acting downstream of R5 neurons in promoting sleep, we performed epistasis experiments. To do this, we first characterized an *R58H05-QF2* line that we generated and found minimal to no labeling of peripheral neurons, expression in the R5 ring with minimal expression in the VNC, and that it induced sleep during and after thermogenetic activation (Figures S3C, S3D, S3F, and S3G). Inhibiting synaptic transmission from EPG neurons markedly suppressed the increased sleep induced by thermogenetic activation of R5 neurons, whereas the sleep amount after activation was not affected (Figures 3G–3I). These findings support a model whereby R5 neurons signal to EPG neurons to promote sleep.

Sleep pressure triggers increased morphological and functional connectivity between R5 and EPG neurons

We previously showed that R5 neurons undergo plastic changes (as measured by an increase in the active zone marker Bruchpilot/BRP) following sleep loss[1]. Thus, we postulated that R5 neuron plasticity may enhance their physical and functional connectivity with EPG neurons. First, we asked whether R5 neurons exhibit morphological changes following SD. We performed single cell dye-fills of R5 neurons using biocytin in the presence and absence of 12 hr SD. Following SD, R5 neurons exhibited a greater number of presynaptic bouton-like puncta, as well as increased thickness of the ring structure in the anterior-to-posterior axis, compared to controls. Importantly, 12 hr recovery sleep reversed these morphological changes (Figures 4A–4E). To examine whether the physical connectivity between the R5 and EPG neurons is influenced by sleep need, GFP Reconstitution Across Synaptic Partners (GRASP)[21] experiments were performed in the presence and absence of SD. While GRASP signal was detected in both 12 hr SD and baseline sleep conditions, the relative GRASP signal between R5 and EPG neurons was significantly increased following SD (Figures 4F–4H). These data suggest that sleep loss triggers structural plasticity in R5 neurons and strengthens physical connectivity between R5 and EPG neurons.

To assess whether these morphological changes produce a functional increase in synaptic strength, we performed dual patch-clamp recordings of R5 and EPG neurons after 12 hrs of SD or baseline sleep. Because the cell bodies of these two groups of neurons are on opposite sides of the fly brain, we developed a novel electrophysiological preparation to conduct these studies, where the brain is mounted vertically (Figure S4A). Owing to their increased excitability following sleep loss[1], smaller currents were injected into R5 neurons in SD brains to yield levels of firing similar to controls (Figure 4I). EPG spike-triggered EPSP

amplitude was significantly increased following SD, compared to controls. Furthermore, in control brains, spike-triggered EPSPs in EPG neurons were observed in only a minority (4/30) of recordings. In contrast, after SD, a greater proportion of brains exhibited a postsynaptic response (8/25) (Figures 4I–4K). To confirm that the EPG membrane potential (Vm) changes were dependent on R5 firing, we compared Vm changes triggered by R5 spikes with those occurring at random. As expected, Vm changes triggered by R5 spikes were significantly larger than background Vm fluctuations, and this difference was greater after SD (Figures S4B–S4D).

We next asked whether cholinergic R5 neurons signal to EPG neurons in our dual patch-clamp recordings. EPG responses to R5 firing were essentially abolished upon application of mecamylamine, a nicotinic acetylcholine receptor antagonist (Figures 4I and 4J), suggesting that cholinergic signaling from R5 neurons triggers excitatory post-synaptic responses in EPG neurons. We next examined unitary EPSPs from EPG neurons following individual R5 spikes. The amplitude of these unitary EPSPs was increased following SD, compared to controls (Figures 4L and 4M), further demonstrating potentiation of R5-EPG synapses with greater sleep need. To assess whether the connection between R5 and EPG is monosynaptic, we quantified EPSP onset times from unitary EPG EPSPs triggered by R5 spikes. The EPSP onset time (~1 ms) was comparable to that reported for monosynaptic connections in the *Drosophila* antennal lobe[22,23] and was not altered by changes in sleep need (Figure 4N). These data demonstrate that sleep loss induces an increase in the likelihood and strength of EPG postsynaptic responses following R5 firing.

Although previous studies have suggested that most EB ring neuron signaling is GABAergic[15,16], cholinergic EB ring subpopulations have been described[24]. Our findings suggest that cholinergic R5 neurons signal to EPG neurons to promote sleep. However, given the modest effects on sleep associated with R5 ChAT knockdown, additional signaling mechanisms likely play a role in this process. Our data further show that sleep loss enhances the anatomical and functional connectivity between R5 and EPG neurons, which appears to be driven primarily by presynaptic plasticity in the R5 neurons. Synaptic plasticity triggered by homeostatic drive is unusual[25,26,27] and may promote persistence of homeostatically-generated behaviors under conditions of significant internal need. Interestingly, while inhibiting EPG neurotransmission largely blocks the sleep-promoting effects of activating R5 neurons, it does not impact the persistent sleep following this activation. This finding suggests that multiple, redundant mechanisms may underlie the sleep persistence phenotype seen with R5 activation.

EPG neurons have been shown to encode directional heading[5,6,9,10,28]. How does one reconcile a role for these neurons in navigation with a potential role in homeostatic sleep regulation? We find that a large number of EPG neurons must be activated to promote sleep behavior. In addition, our dual patch-clamp recordings reveal that, not only does the synaptic strength between R5 and EPG neurons increase with greater sleep need, but also the proportion of these functional connections. Thus, we speculate that the R5/EPG synapse acts as a “gate” for transmission of homeostatic sleep drive. In this model, under baseline conditions, EPG neurons function as compass neurons and receive broad, inhibitory inputs[29,30] and weak and infrequent excitatory R5 inputs. Following sleep deprivation,

plasticity of R5 neurons is induced[1,31], enhancing R5→EPG excitatory signaling. Moreover, sleep loss promotes synchronization of R5 neuron activity[32], which could further strengthen and coordinate sleep need-dependent R5 signaling to EPG neurons. These changes could lead to activation of a greater number of EPG neurons and promote recovery sleep.

STAR Methods

RESOURCE AVAILABILITY

Lead Contact—Further information and requests for data, resources and reagents should be directed to and will be fulfilled by the Lead Contact, Dr. Mark N. Wu (marknwu@jhmi.edu).

Materials Availability—Transgenic *Drosophila* strains generated for this manuscript are available upon request to the lead contact.

Data and Code Availability

- Raw data, analysis files, and images generated for this manuscript are available upon request to the lead contact.
- Jupyter notebooks are available upon request from the lead contact. Additional code for this manuscript is available on Github (https://github.com/margiezilla/Ho_etal_2022).
- Any additional information required to reanalyze the data reported in this paper is available from the lead contact upon request.

EXPERIMENTAL MODEL AND SUBJECT DETAILS

Adult female *Drosophila melanogaster* of age 4–10 days old were used for all experiments. Flies were reared on standard food containing molasses, cornmeal, and yeast under a 12:12 h LD cycle at 25°C, with the exception of crosses utilizing dTRPA1 (in which case flies were reared at 23°C).

METHOD DETAILS

Transgenic Fly Strains—All GMR GAL4 and LexA lines were obtained from the Bloomington *Drosophila* Stock Center[36,37]. Other flies were obtained as described in the Key Resources Table.

Molecular Biology—The ChAT microRNA (miR) was constructed as previously described[38]. For *UAS-ChaT-miR*, two 22-mers in exon 4 (5'-ACCGCTGGCTGGGAACTTTAAT-3') and exon 7 (5'-AGATGCACGAGCTGTTCAAAGA-3') were used to create the two hairpin loops. The miR sequence was synthesized *in vitro* (GeneArt) and subcloned into pUAST using *EcoRI* and *NotI*. The *UAS-ChAT-miR1-A* line was generated via random P-element mediated insertion into *iso31* flies and screened for viability and general health. The *R58H05-QF2-7* line was as described in Blum et al., 2021[2]. The *R58H05-QF2-A* line was generated by re-injecting the construct into *iso31* flies using P-element mediated random insertion and was selected to

avoid expression in peripheral tissues. The *R58H05-p65AD* and *R46C03-GAL4 DBD* lines were generated as described in Blum et al., 2021[2].

Immunostaining—Neurotransmitter immunostaining was performed as previously described[16]. The following primary antibodies were used: rabbit-anti-GABA (1:500, Sigma, A2052, RRID: AB_477652), mouse-anti-ChAT (1:100, DSHB 4B1, RRID: AB_528122), and rabbit-anti-vGluT (1:5000, RRID: AB_2567386). Secondary antibodies were raised in goat against rabbit, chicken and mouse antisera (Invitrogen) and conjugated to Alexa Fluor 488 (1:1000), Alexa Fluor 555 (1:1000) or Alexa Fluor 647 (1:300). Antibodies were prepared in blocking buffer with 0.02% NaN_3, and primary antibodies were reused several times. Whole mount brain immunostaining for other antigens was performed as previously described[16]. The following primary antibodies were used: chicken-anti-GFP (1:1000, Invitrogen A10262, RRID:AB_2534023), rabbit-anti-dsRed (1:1000, Clontech, 632496, RRID: AB_10013483) and mouse-anti-BRP (1:10, DSHB nc82, RRID: AB_2314866). Secondary antibodies were raised in goat against chicken, rabbit, or mouse antisera (Invitrogen) and conjugated to Alexa Fluor 488 (1:1000), or Alexa Fluor 568 (1:1000) or Alexa Fluor 647 (1:300). For counting putative EPG cells labeled by various drivers in Figure S1J, single or combined transgenic driver lines were used to express mCD8::GFP, and immunostaining was performed as described. GFP^+ cells with expected projections to the PB were counted as EPG cells. In addition, in cases where their projections could not be clearly visualized, GFP^+ cells of similar size immediately surrounding those cells were counted as putative EPG neurons. To quantify ChAT knockdown in Figure S3A, a single Z-slice (1 μm) that captured the thickest portion of the mushroom body γ-lobe was chosen for analysis. Using ImageJ, a region of interest (ROI) was drawn around a single γ-lobe per brain, and the average fluorescence intensity was measured.

Behavioral measurements—Strains used in behavioral experiments were outcrossed at least four times to *iso31* background (RRID: BDSC_5905), and 5–8 day old female flies were used for all behavioral experiments. Sleep behavior was measured using the *Drosophila* Activity Monitoring system (Trikinetics) and established metrics as previously described[39]. Sleep parameters were analyzed using custom MATLAB scripts[2], and additional post-processing analysis was performed with Python using Jupyter notebook (https://github.com/margiezilla/Ho_etal_2022). Flies were loaded in sucrose locomotor tubes (5% sucrose, 2% agar) for all behavioral experiments. For *UAS-dTRPA1* experiments, adult flies were raised at 23°C. 1 day of baseline sleep was recorded at 22°C and then the temperature was raised to 29°C during ZT12-24 during the second night. The temperature was returned to 22°C starting at ZT0 the following day. For arousal threshold measurements during dTRPA1 activation at 29C, flies were subjected to stimuli of increasing intensity and duration using a digital vortexer (500RPM for 1s (0.2g), 2s (0.25g), and 4s (0.35g) at ZT16, ZT18, ZT20 and ZT22). Asleep flies were defined as flies not moving for the 5 minutes (no beam crosses detected) prior to stimulus, whereas awake flies were those observed to be moving. Aroused flies were identified as flies moving within the 3 min interval following the stimulus. For sleep deprivation experiments, adult flies were raised at 25°C and assayed at 25°C. Sleep deprivation was performed by mechanical stimulation, by shaking 2–3 sec/minute in a digital vortexer (VWR DVX-2500 Multi-tube vortexer) at 1300–2000 RPM

from ZT12-24. Homeostatic sleep rebound from the following 6 hours (ZT0-6) was then recorded and compared to previous daytime sleep to calculate rebound sleep. Only flies exhibiting ≥95% sleep deprivation were used in analyses. Locomotor climbing performance following thermogenetic activation of EPG neurons was performed essentially as previously described[40,41]. 10–12 flies (5 days old) were exposed to 29°C for 2 hrs (ZT0-2) and then tapped to the bottom of a clean plastic vial with another vial placed above. The proportion of flies climbing above a 10 cm mark was measured after 10 s. To assess peak locomotor activity during thermogenetic activation of EPG neurons, we measured the maximum number of beam crossings within 1 min for the 5 min window immediately following the strong shaking stimuli shown in Figures 1D and 1E.

Single cell dye labeling of R5 neurons.—Single cell dye labeling of R5 neurons was performed by iontophoretic injection of biocytin for at least 15 min in order to quantify the puncta number and ring thickness of an R5 neuron. After iontophoretic injection of biocytin, the brain was fixed in 4% paraformaldehyde in Phosphate Buffered Saline (PBS, 137 mM NaCl, 2.7 mM KCl, 10 mM Na_2HPO_4, 1.7 mM KH_2PO_4, pH 7.4) overnight at 4°C. After washing for 1 hr in several changes of PBST (0.3% Triton X-100 in PBS) at room temperature, the brain was incubated with rabbit anti-GFP antibodies (Thermo Fisher A11122, 1:200) for 16–40 hrs on a shaker at 4°C, followed by incubation with fluorescent Alexa Fluor 488 anti-rabbit (Thermo Fisher A27034, 1:1000) secondary antibodies and Alexa 568-conjugated streptavidin (Thermo Fisher S11226, 1:100) for 24–40 hrs on a shaker at 4°C. After a 1 hr wash, samples were cleared in 70% glycerol in PBS for 5 min at room temperature and then mounted in Vectashield (Vector Labs). Brains were then imaged using a confocal imaging system (LSM-700; Carl Zeiss). Serial optical sections were acquired at 0.7–1.0 μm intervals.

To quantify spot number and ring thickness of dye-injected R5 neurons, we used Imaris image analysis software (Imaris x64 9.7.1, Oxford instruments). To measure spot number, we first manually measured representative spot diameter and applied this variable as the “Estimated Diameter.” We selected “quality” as the filter type for our analysis. We then manually tuned the quality parameter until every punctate region of interest on the R5 axonal ring was covered by a spot. Typically, only a single class (“Class A”) was generated based on the average distance to 3 nearest neighbors, but if the algorithms returned more than one class (e.g. “Class A” and “Class B”), only class A was selected for analysis because other classes were below the distance threshold (i.e, too close together). Finally, we manually removed spots outside the R5 ring structure and selected “Total Number of Spots” as the output.

To measure anterior-posterior R5 ring thickness, we used the “Measurement Points” function in Imaris. We selected the thickest area of the structure and quantified anterior-posterior thickness with measurement points on the anterior and posterior surfaces. To ensure the only difference in measurement was on the z-axis, we synchronized the x- and y-axis of the two points

Connectivity using GRASP—GRASP[21] was used to assess physical connectivity between R5 and EPG neurons. The *R30G03-p65AD*; *R58H05-DBD* and *R19G02-LexA*

were used to drive expression of *UAS-CD4-spGFP1-10* in R5 neurons and *LexAop-CD4-spGFP11* and *LexAop-tdTomato* in EPG neurons, respectively. These flies were subjected to mechanical SD or undisturbed (non-SD) from ZT12-24 as described above. The brains of SD and non-SD control flies were quickly dissected in cold AHLS (2 mM $CaCl_2$, 108 mM NaCl, 5 mM KCl, 8.2 mM $MgCl_2$, 4 mM $NaHCO_3$, 1 mM NaH_2PO_4, 5 mM HEPES, 10 mM Sucrose, 5 mM Trehalose, pH 7.5) and native GFP fluorescence was imaged with confocal microscopy (Zeiss LSM700) using a 63x oil immersion objective. Relative quantification of GRASP fluorescence levels was performed by measuring GFP signal against tdTomato. Stacks containing the EB region labeled by tdTomato signal were projected into images by using the "average intensity" function in ImageJ. The ROI was also determined by tdTomato signal labeling the EB neuropil. The "Analyze -> Measure" function of ImageJ was used to quantify the GFP and tdTomato fluorescence intensity in the ROI.

Electrophysiological recordings—The procedures were performed as previously described[42]. Sleep deprivation was performed using mechanical stimulation with a multi-tube digital vortexer (VWR VX-2500) at 5 s/min from ZT12-ZT24, and flies with >90% sleep loss during this period were used for electrophysiological recordings. Recordings were performed at ZT0-3.

***ex vivo* preparation—**Flies were chilled on ice for anesthesia and immobilized on a dissecting chamber following isolation of the head. The brain was exposed by opening the head capsule and dissected in a *Drosophila* physiological saline solution (101 mM NaCl, 3 mM KCl, 1 mM $CaCl_2$, 4 mM $MgCl_2$, 1.25 mM NaH_2PO_4, 20.7 mM $NaHCO_3$, and 5 mM glucose; pH 7.2). The tracheae and the intracranial muscles were removed. To better visualize the recording site and increase the likelihood of a successful recording, the glial sheath surrounding the brain was focally and carefully removed after treating with an enzymatic cocktail, collagenase (0.2 mg/mL), protease XIV (0.4 mg/mL), and dispase (0.6 mg/mL), at 22°C for 1–2 min. The surface of the cell body was briefly cleaned with a small stream of saline that was pressure-ejected from a large-diameter pipette under visualization of a dissecting microscope. For dual recordings of R5 and EPG neurons, brains were mounted vertically to allow electrode access from both anterior and posterior sides. Brains were vertically immobilized on the bottom of the recording chamber, by placing dental wax (GC Corp., 27B2X00008000016) in front of and behind the brain.

Perforated patch-clamp recordings—Glass pipettes (8–12 MΩ) were fashioned from borosilicate capillaries with a Flaming/Brown puller (P-1000; Sutter Instrument). A final concentration of 50 μM escin (Santa Cruz Biotechnology) was added fresh into the internal pipette solution (102 mM potassium gluconate, 0.085 mM $CaCl_2$, 0.94 mM EGTA, 8.5 mM HEPES, 4 mM Mg-ATP, 0.5mM Na-GTP, 17 mM NaCl; pH7.2). Because escin is light-sensitive, filling syringes were wrapped with aluminum foil. Pipette tips were dipped briefly for 1 s or less into a small container with escin-free internal pipette solution, and then were back-filled with the escin-containing solution from the filling syringe. 50 μM mecamylamine was used to isolate the cells from excitatory synaptic inputs for the experiments with pharmacological blockade. Perforated patches could develop spontaneously over time

(usually ~1–8 min) without any suction pulse applied in the pipette. Single electrode recordings from EPG neurons were acquired with an Axopatch 200B amplifier (Molecular Devices), and dual recordings from R5 and EPG neurons were performed using two patch-clamp amplifiers–an Axopatch 200B amplifier and a Model 2400 amplifier with 100 MΩ headstage (A-M systems). The voltage signals were sampled at 20 kHz and lowpass filtered at 2 kHz.

Electrophysiology data analysis—To quantify spontaneous excitatory postsynaptic potentials (sEPSPs) from EPG neurons under single electrode current-clamp recording configuration, a median filter with a time constant of 3 ms was applied to the unfiltered membrane potential. Then, background noise power was computed based on root mean square values from the all-points amplitude in each dataset. These computations were used to define noise-rejection criteria to decide signal threshold[27]. Once sEPSPs were sorted, their amplitude was then defined as the difference between the maximum/minimum potential of each sEPSP. EPSP-spike coupling was defined as temporal distance between adjacent presynaptic R5 action potential (AP, preceding) and EPG EPSP (following) epochs. To examine the functional connectivity between R5 and EPG neurons under dual electrode current-clamp recording configuration, depolarizing current injections were applied to R5 cells to evoke spike trains, and the membrane potentials of EPG were simultaneously recorded. The change in EPG membrane voltage was calculated by subtracting the mean membrane potential before current injection from the mean membrane potential during the period of current injection. We carefully modulated the amount of injected current in every experiment so that we could induce a similar number of action potentials between R5 with and without sleep deprivation. This is particularly important, because the membrane excitability of R5 is increased after sleep deprivation[1]. Within the “responding” paired recordings, we sorted a 30 ms time window of membrane voltage traces for EPG centered on a simultaneously measured R5 spike to assess for a monosynaptic interaction between R5 and EPG neurons. By performing visual inspection, the sorted EPG membrane voltages were further categorized into detectable or undetectable unitary EPSPs based on the presence of a clear depolarization (typically >0.2 mV), as well as monotonic rise time kinetics and phase-locked latency indicating monosynaptic excitation. The sorted EPG membrane voltages categorized as detectable were quantified in their amplitudes of peak depolarization. To exclude the possibility that detected depolarization could be coincidentally observed in the absence of R5 spike events, we also quantified randomly chosen 30 ms membrane voltage traces of EPG and confirmed that there was no detectable depolarization. The monosynaptic EPSP onset time[43] was defined as the time from the peak of R5 AP to the time reaching 10% of the peak depolarization after R5 AP. All analyses were performed using MATLAB (The MathWorks).

Quantification and Statistical Analysis—Statistical analyses were performed with Prism (GraphPad). For comparisons of two groups of normally distributed data, Student’s t tests were performed. For multiple comparisons of normally-distributed data, one-way or two-way ANOVAs followed by Tukey’s post-hoc tests were performed. For multiple comparison of non-normally distributed data, Kruskal-Wallis test followed by Dunn’s post-hoc test was performed.

Supplementary Material

Refer to Web version on PubMed Central for supplementary material.

Acknowledgments

We thank T. Wolff, W. Joiner, V. Jayaraman, and G. Rubin (HHMI Janelia) for kindly sharing reagents. We thank A. Hutson, Y. Zhang, and Y. Xie for assistance with Imaris imaging and I.D. Blum for assistance with sleep behavior analysis. We thank the Bloomington Stock Center (supported by NIH grant P40OD018537) and the Vienna *Drosophila* Stock Center (www.vdrc.at) for fly stocks. This work was supported by NINDS Center Grant P30 BNS050274 for use of the Core Machine Shop and the Multiphoton Imaging Core, ERC Starting Grant 758580 (S.L.), the Howard Hughes Medical Institute (A.L.K.), and NIH grants K99NS117654 (M.C.W.H.), K99NS101065 (M.T.), F31NS117175 (M.B.), R01NS100792 (M.N.W.), and R35NS122181 (M.N.W.).

Inclusion and Diversity

We support inclusive, diverse, and equitable conduct of research.

References

1. Liu S, Liu Q, Tabuchi M, and Wu MN (2016). Sleep Drive Is Encoded by Neural Plastic Changes in a Dedicated Circuit. Cell 165, 1347–1360. 10.1016/j.cell.2016.04.013. [PubMed: 27212237]
2. Blum ID, Keles MF, Baz ES, Han E, Park K, Luu S, Issa H, Brown M, Ho MCW, Tabuchi M, et al. (2021). Astroglial Calcium Signaling Encodes Sleep Need in *Drosophila*. Current biology : CB 31, 150–162 e157. 10.1016/j.cub.2020.10.012. [PubMed: 33186550]
3. Scheffer LK, Xu CS, Januszewski M, Lu Z, Takemura SY, Hayworth KJ, Huang GB, Shinomiya K, Maitlin-Shepard J, Berg S, et al. (2020). A connectome and analysis of the adult *Drosophila* central brain. Elife 9. 10.7554/eLife.57443.
4. Hulse BK, Haberkern H, Franconville R, Turner-Evans DB, Takemura SY, Wolff T, Noorman M, Dreher M, Dan C, Parekh R, et al. (2021). A connectome of the *Drosophila* central complex reveals network motifs suitable for flexible navigation and context-dependent action selection. Elife 10. 10.7554/eLife.66039.
5. Seelig JD, and Jayaraman V (2015). Neural dynamics for landmark orientation and angular path integration. Nature 521, 186–191. 10.1038/nature14446. [PubMed: 25971509]
6. Green J, Adachi A, Shah KK, Hirokawa JD, Magani PS, and Maimon G (2017). A neural circuit architecture for angular integration in *Drosophila*. Nature 546, 101–106. 10.1038/nature22343. [PubMed: 28538731]
7. Nicolai LJ, Ramaekers A, Raemaekers T, Drozdzecki A, Mauss AS, Yan J, Landgraf M, Annaert W, and Hassan BA (2010). Genetically encoded dendritic marker sheds light on neuronal connectivity in *Drosophila*. Proceedings of the National Academy of Sciences of the United States of America 107, 20553–20558. [PubMed: 21059961]
8. Zhang YQ, Rodesch CK, and Broadie K (2002). Living synaptic vesicle marker: synaptotagmin-GFP. Genesis 34, 142–145. 10.1002/gene.10144. [PubMed: 12324970]
9. Wolff T, Iyer NA, and Rubin GM (2015). Neuroarchitecture and neuroanatomy of the *Drosophila* central complex: A GAL4-based dissection of protocerebral bridge neurons and circuits. The Journal of comparative neurology 523, 997–1037. 10.1002/cne.23705. [PubMed: 25380328]
10. Wolff T, and Rubin GM (2018). Neuroarchitecture of the *Drosophila* central complex: A catalog of nodulus and asymmetrical body neurons and a revision of the protocerebral bridge catalog. The Journal of comparative neurology 526, 2585–2611. 10.1002/cne.24512. [PubMed: 30084503]
11. Nern A, Pfeiffer BD, and Rubin GM (2015). Optimized tools for multicolor stochastic labeling reveal diverse stereotyped cell arrangements in the fly visual system. Proceedings of the National Academy of Sciences of the United States of America 112, E2967–2976. 10.1073/pnas.1506763112. [PubMed: 25964354]

12. Meissner GW, Dorman Z, Nern A, Forster K, Gibney T, Jeter J, Johnson L, He Y, Lee K, Melton B, et al. (2020). An image resource of subdivided *Drosophila* GAL4-driver expression patterns for neuron-level searches. bioRxiv. 10.1101/2020.05.29.080473.
13. Konig P, Engel AK, and Singer W (1996). Integrator or coincidence detector? The role of the cortical neuron revisited. Trends in neurosciences 19, 130–137. 10.1016/s0166-2236(96)80019-1. [PubMed: 8658595]
14. Zsiros V, and Hestrin S (2005). Background synaptic conductance and precision of EPSP-spike coupling at pyramidal cells. Journal of neurophysiology 93, 3248–3256. 10.1152/jn.01027.2004. [PubMed: 15716369]
15. Kahsai L, Carlsson MA, Winther AM, and Nassel DR (2012). Distribution of metabotropic receptors of serotonin, dopamine, GABA, glutamate, and short neuropeptide F in the central complex of *Drosophila*. Neuroscience 208, 11–26. 10.1016/j.neuroscience.2012.02.007. [PubMed: 22361394]
16. Xie X, Tabuchi M, Brown MP, Mitchell SP, Wu MN, and Kolodkin AL (2017). The laminar organization of the *Drosophila* ellipsoid body is semaphorin-dependent and prevents the formation of ectopic synaptic connections. Elife 6. 10.7554/eLife.25328.
17. Diao F, Ironfield H, Luan H, Diao F, Shropshire WC, Ewer J, Marr E, Potter CJ, Landgraf M, and White BH (2015). Plug-and-play genetic access to *Drosophila* cell types using exchangeable exon cassettes. Cell reports 10, 1410–1421. 10.1016/j.celrep.2015.01.059. [PubMed: 25732830]
18. Satterfield LK, De J, Wu M, Qiu T, and Joiner WJ (2022). Inputs to the sleep homeostat originate outside the brain. The Journal of neuroscience : the official journal of the Society for Neuroscience. 10.1523/JNEUROSCI.2113-21.2022.
19. Shimono K, Fujimoto A, Tsuyama T, Yamamoto-Kochi M, Sato M, Hattori Y, Sugimura K, Usui T, Kimura K, and Uemura T (2009). Multidendritic sensory neurons in the adult *Drosophila* abdomen: origins, dendritic morphology, and segment- and age-dependent programmed cell death. Neural Dev 4, 37. 10.1186/1749-8104-4-37. [PubMed: 19799768]
20. Seidner G, Robinson JE, Wu M, Worden K, Masek P, Roberts SW, Keene AC, and Joiner WJ (2015). Identification of Neurons with a Privileged Role in Sleep Homeostasis in *Drosophila melanogaster*. Current biology : CB 25, 2928–2938. 10.1016/j.cub.2015.10.006. [PubMed: 26526372]
21. Gordon MD, and Scott K (2009). Motor control in a *Drosophila* taste circuit. Neuron 61, 373–384. [PubMed: 19217375]
22. Kazama H, and Wilson RI (2008). Homeostatic matching and nonlinear amplification at identified central synapses. Neuron 58, 401–413. 10.1016/j.neuron.2008.02.030. [PubMed: 18466750]
23. Huang J, Zhang W, Qiao W, Hu A, and Wang Z (2010). Functional connectivity and selective odor responses of excitatory local interneurons in *Drosophila* antennal lobe. Neuron 67, 1021–1033. 10.1016/j.neuron.2010.08.025. [PubMed: 20869598]
24. Martin-Pena A, Acebes A, Rodriguez JR, Chevalier V, Casas-Tinto S, Triphan T, Strauss R, and Ferrus A (2014). Cell types and coincident synapses in the ellipsoid body of *Drosophila*. The European journal of neuroscience 39, 1586–1601. 10.1111/ejn.12537. [PubMed: 24605774]
25. Kong D, Dagon Y, Campbell JN, Guo Y, Yang Z, Yi X, Aryal P, Wellenstein K, Kahn BB, Sabatini BL, and Lowell BB (2016). A Postsynaptic AMPK-->p21-Activated Kinase Pathway Drives Fasting-Induced Synaptic Plasticity in AgRP Neurons. Neuron 91, 25–33. 10.1016/j.neuron.2016.05.025. [PubMed: 27321921]
26. Liu T, Kong D, Shah BP, Ye C, Koda S, Saunders A, Ding JB, Yang Z, Sabatini BL, and Lowell BB (2012). Fasting activation of AgRP neurons requires NMDA receptors and involves spinogenesis and increased excitatory tone. Neuron 73, 511–522. 10.1016/j.neuron.2011.11.027. [PubMed: 22325203]
27. Liu Q, Tabuchi M, Liu S, Kodama L, Horiuchi W, Daniels J, Chiu L, Baldoni D, and Wu MN (2017). Branch-specific plasticity of a bifunctional dopamine circuit encodes protein hunger. Science 356, 534–539. 10.1126/science.aal3245. [PubMed: 28473588]
28. Seelig JD, and Jayaraman V (2013). Feature detection and orientation tuning in the *Drosophila* central complex. Nature 503, 262–266. 10.1038/nature12601. [PubMed: 24107996]

29. Flores-Valle A, Goncalves PJ, and Seelig JD (2021). Integration of sleep homeostasis and navigation in *Drosophila*. PLoS Comput Biol 17, e1009088. 10.1371/journal.pcbi.1009088. [PubMed: 34252086]
30. Kim SS, Rouault H, Druckmann S, and Jayaraman V (2017). Ring attractor dynamics in the *Drosophila* central brain. Science 356, 849–853. 10.1126/science.aal4835. [PubMed: 28473639]
31. Huang S, Piao C, Beuschel CB, Gotz T, and Sigrist SJ (2020). Presynaptic Active Zone Plasticity Encodes Sleep Need in *Drosophila*. Current biology : CB 30, 1077–1091 e1075. 10.1016/j.cub.2020.01.019. [PubMed: 32142702]
32. Raccuglia D, Huang S, Ender A, Heim MM, Laber D, Suarez-Grimalt R, Liotta A, Sigrist SJ, Geiger JRP, and Owald D (2019). Network-Specific Synchronization of Electrical Slow-Wave Oscillations Regulates Sleep Drive in *Drosophila*. Current biology : CB 29, 3611–3621 e3613. 10.1016/j.cub.2019.08.070. [PubMed: 31630955]
33. Daniels RW, Gelfand MF, Collins CA, and DiAntonio A (2008). Visualizing glutamatergic cell bodies and synapses in *Drosophila* larval and adult CNS. J Comp Neurol 508, 131–152. [PubMed: 18302156]
34. Pfeiffer BD, Truman JW, and Rubin GM (2012). Using translational enhancers to increase transgene expression in *Drosophila*. Proceedings of the National Academy of Sciences of the United States of America 109, 6626–6631. 10.1073/pnas.1204520109. [PubMed: 22493255]
35. Brand AH and Perrimon N (1993). Targeted gene expression as a means of altering cell fates and generating dominant phenotypes. Development 118, 401–415. [PubMed: 8223268]
36. Pfeiffer BD, Jenett A, Hammonds AS, Ngo TT, Misra S, Murphy C, Scully A, Carlson JW, Wan KH, Laverty TR, et al. (2008). Tools for neuroanatomy and neurogenetics in *Drosophila*. Proceedings of the National Academy of Sciences of the United States of America 105, 9715–9720. [PubMed: 18621688]
37. Jenett A, Rubin GM, Ngo TT, Shepherd D, Murphy C, Dionne H, Pfeiffer BD, Cavallaro A, Hall D, Jeter J, et al. (2012). A GAL4-driver line resource for *Drosophila* neurobiology. Cell reports 2, 991–1001. [PubMed: 23063364]
38. Chen CH, Huang H, Ward CM, Su JT, Schaeffer LV, Guo M, and Hay BA (2007). A synthetic maternal-effect selfish genetic element drives population replacement in *Drosophila*. Science 316, 597–600. [PubMed: 17395794]
39. Shaw PJ, Cirelli C, Greenspan RJ, and Tononi G (2000). Correlates of sleep and waking in *Drosophila melanogaster*. Science 287, 1834–1837. [PubMed: 10710313]
40. Crowther DC, Kinghorn KJ, Miranda E, Page R, Curry JA, Duthie FA, Gubb DC, and Lomas DA (2005). Intraneuronal Abeta, non-amyloid aggregates and neurodegeneration in a *Drosophila* model of Alzheimer's disease. Neuroscience 132, 123–135. [PubMed: 15780472]
41. Woolums BM, McCray BA, Sung H, Tabuchi M, Sullivan JM, Ruppell KT, Yang Y, Mamah C, Aisenberg WH, Saavedra-Rivera PC, et al. (2020). TRPV4 disrupts mitochondrial transport and causes axonal degeneration via a CaMKII-dependent elevation of intracellular Ca(2). Nat Commun 11, 2679. 10.1038/s41467-020-16411-5. [PubMed: 32471994]
42. Tabuchi M, Monaco JD, Duan G, Bell B, Liu S, Liu Q, Zhang K, and Wu MN (2018). Clock-Generated Temporal Codes Determine Synaptic Plasticity to Control Sleep. Cell 175, 1213–1227 e1218. 10.1016/j.cell.2018.09.016. [PubMed: 30318147]
43. Wilson RI, Turner GC, and Laurent G (2004). Transformation of olfactory representations in the *Drosophila* antennal lobe. Science 303, 366–370. 10.1126/science.1090782. [PubMed: 14684826]

Highlights

- Broad activation of EPG compass neurons promotes sleep in *Drosophila*
- EPG activity increases with sleep need and facilitates homeostatic sleep rebound
- R5 sleep drive neurons act upstream of EPG neurons
- Sleep loss strengthens R5/EPG connectivity to enhance transmission of sleep drive

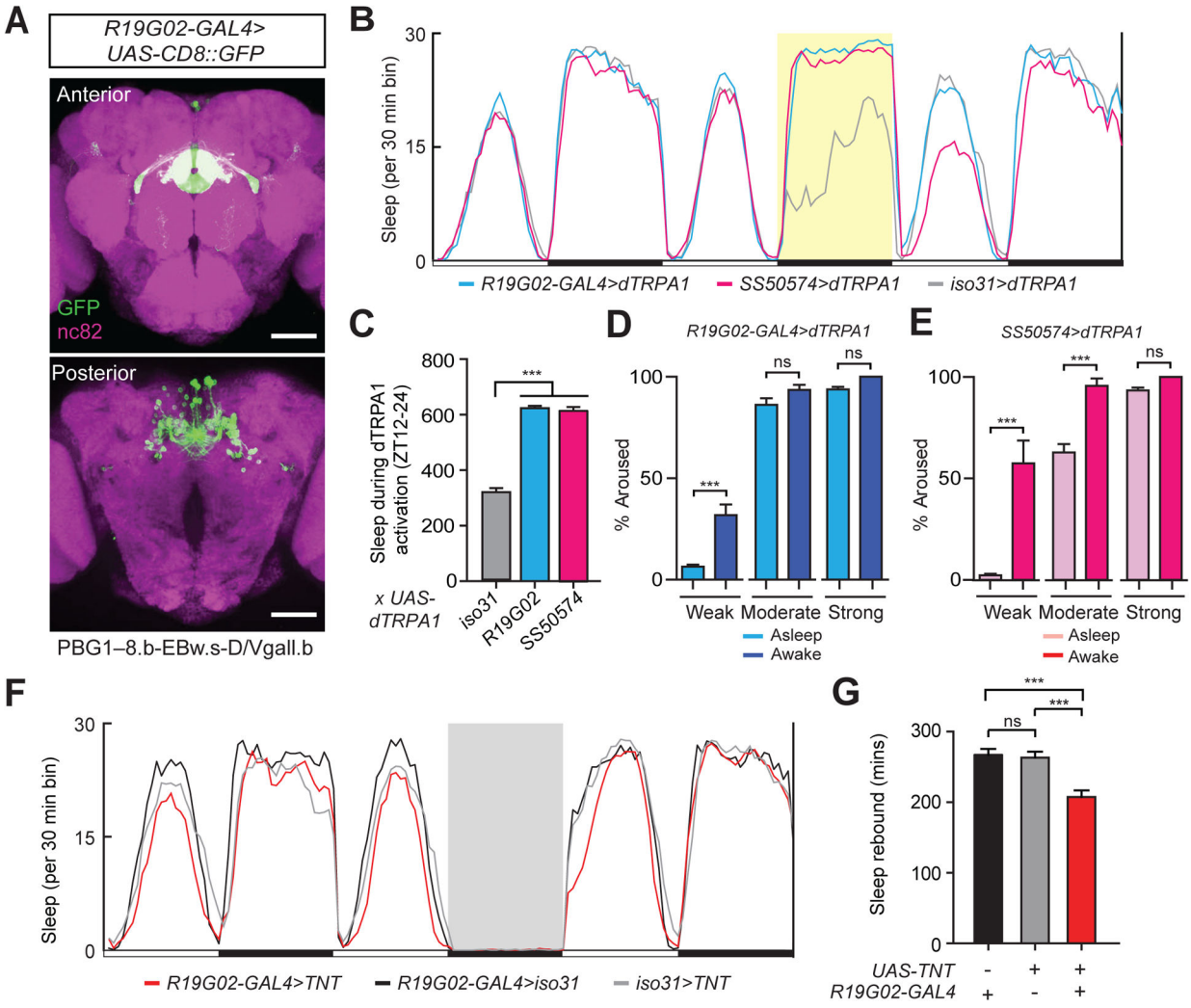

Figure 1. A sleep-promoting role for EPG neurons

(A) Immunostaining of EPG neurons. Whole-mount brain immunostaining of an *R19G02-GAL4>UAS-CD8::GFP* animal with anti-GFP (green) and anti-Bruchpilot (BRP, nc82, magenta) antibody staining. Maximal intensity projection of the central brain is shown. Scale bar indicates 50 μm.

(B) Sleep profiles of *R19G02-GAL4>dTRPA1* (blue), *SS50574>dTRPA1* (magenta), and *iso31>dTRPA1* (gray) flies. Sleep time plotted in 30 min bins. White and black bars indicate 12 hr light and dark periods, respectively. The period of 12hr dTRPA1 activation at 29°C is indicated with a yellow background. Data are from same animals as in (C).

(C) Sleep amount during 12h dTRPA1 activation for *iso31>dTRPA1* (n=96), *R19G02-GAL4>dTRPA1* (n=96), and *SS50574>dTRPA1* (n=93) flies. Mean ± SEM is shown; one way ANOVA with Tukey's post-hoc test.

(D and E) Arousal threshold is increased during EPG neuron activation. The percentage of *R19G02-GAL4>dTRPA1* (D) or *SS50574-GAL4>dTRPA1* (E) flies undergoing 12h dTRPA1 activation at 29°C that were asleep (light blue or light magenta) or awake (dark blue or dark magenta) aroused by weak (0.2 g, n=116 and 152), moderate (0.25 g, n=155 and 171), and strong (0.35 g, n=139 and 140) mechanical rotational stimuli at ZT16, ZT18,

ZT20, and ZT22. Mean ± SEM is shown; Student's t test for each stimulus condition, with Bonferroni correction.

(F) Sleep profiles of *R19G02-GAL4>UAS-TNT* (red), *R19G02-GAL4>iso31* (black), and *iso31>UAS-TNT* (gray) flies. Sleep time plotted in 30 min bins. White and black bars indicate 12 hr light and dark periods, respectively. The period of sleep deprivation via mechanical shaking is indicated with a gray background. Data are from same animals as in (G).

(G) Rebound sleep following deprivation from ZT0-6 for *R19G02-GAL4>iso31* (n=62), *iso31>UAS-TNT* (n=90), and *R19G02-GAL4>UAS-TNT* (n=81) flies. Mean ± SEM is shown; one way ANOVA with Tukey's post hoc test. In this and in subsequent figures *, **, ***, and ns denote $P<0.05$, $P<0.01$, $P<0.001$, and not significant, respectively. See also Figure S1 and Table S1.

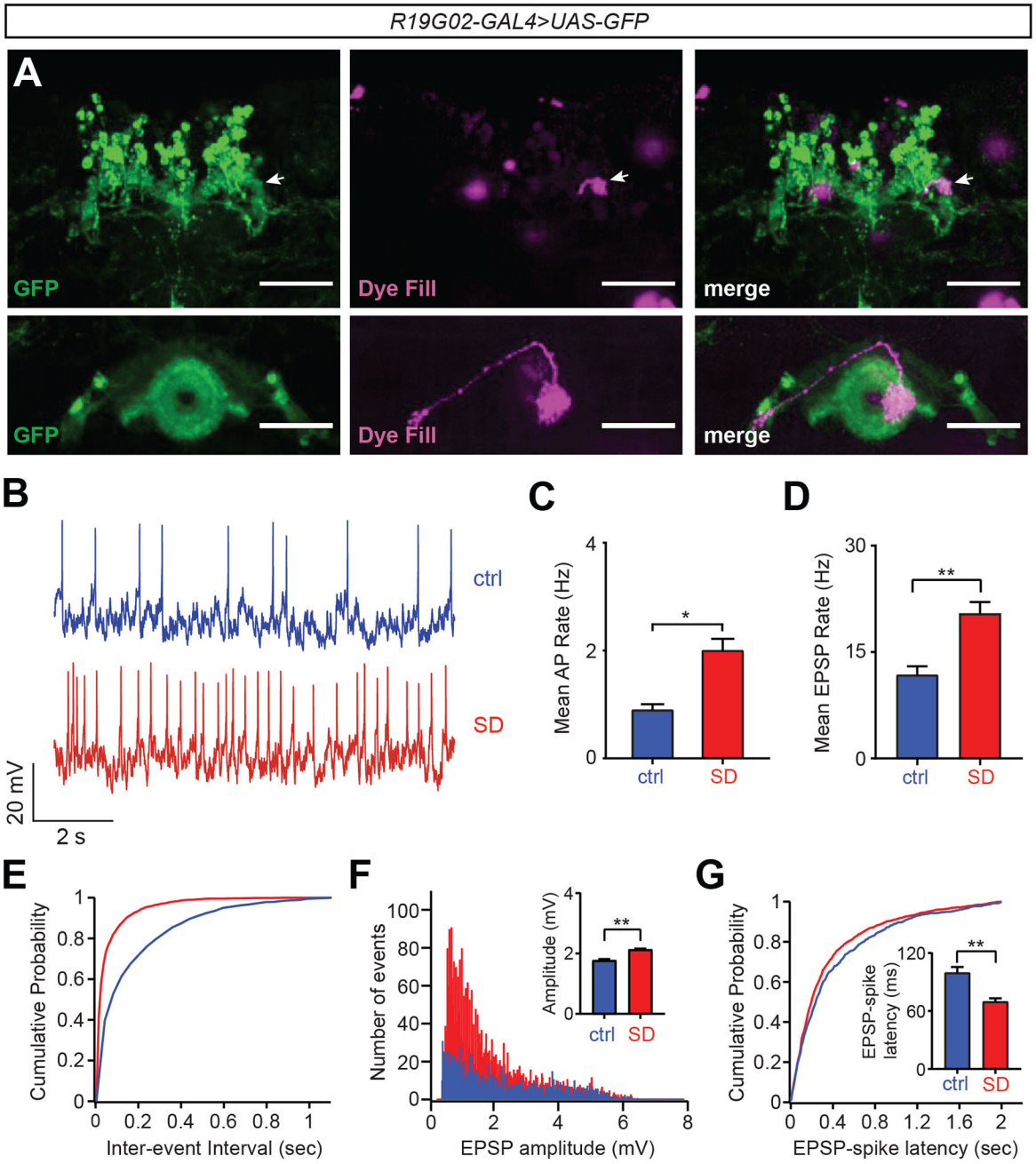

Figure 2. EPG neuron activity is increased with greater sleep need

(A) Whole-mount brain immunostaining of *R19G02-GAL4>UAS-CD4::tdGFP* animal with anti-GFP (green) and single cell dye fill (biocytin, magenta) following electrophysiological measurements demonstrating labeling of EPG projections. Arrows point to dye-filled terminal overlapping GFP signal in the PB. Scale bar, 50 um.

B) Representative traces of membrane potentials of EPG neurons from *R19G02-GAL4>UAS-CD4::tdGFP* flies at ZT0-ZT3 in the presence and absence of 12 hr sleep deprivation (SD).

(C and D) Mean spontaneous action potential (AP) frequency (C) or mean spontaneous excitatory postsynaptic potential (sEPSP) frequency (D) of EPG neurons (*R19G02-GAL4>UAS-CD4::tdGFP*) at ZT0-3 (blue, n=5) and ZT0-3 with SD (red, n=4) flies; Student's t-test.

(E) Cumulative probability plot of spontaneous excitatory postsynaptic potential (sEPSP) frequency from EPG neurons following SD (red) vs control without SD (blue).

(F) Distribution and quantification (inset) of sEPSP peak amplitude from EPG neurons in the presence (red) and absence (blue) of SD; Student's t-test.

(G) Cumulative probability plot and quantification (inset) of EPSP-spike latencies for EPG neurons in ctrl (blue) vs SD (red) flies; Student's t-test. Data in panels (C–G) are from the same flies. See also Figure S2.

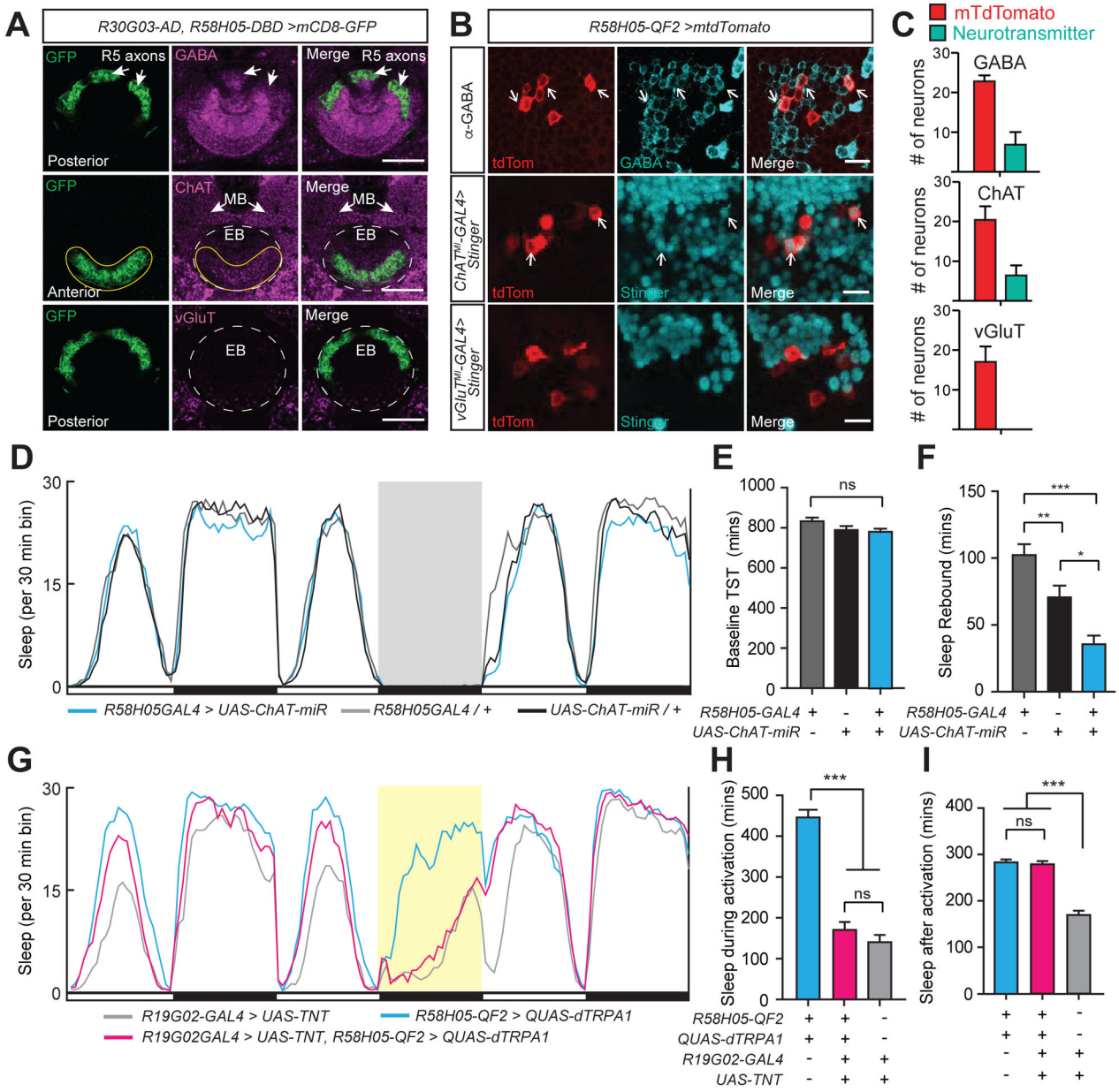

Figure 3. R5 neurons act upstream of EPG neurons to promote sleep

(A) Neurotransmitter staining of R5 ring neurons in an *R30G03-AD, R58H05-DBD>UAS-mCD8::GFP* animal. Whole-mount brain immunostaining showing anti-GFP (green), either anti-GABA, anti-ChAT, or anti-VGluT (magenta), and merged signals. Top row, posterior aspect, arrows indicate co-localization of R5 axons with GABA signal. Middle row, anterior aspect, ChAT staining colocalization with GFP signal is indicated (yellow solid line), while the location of EB ring is shown with white dashed lines. Arrows point to mushroom body (MB) lobes. Bottom, posterior aspect, no detectable overlap between vGLUT expression and GFP. EB ring is outlined with white dashed lines. Scale bars indicate 20 μm.

(B) Co-staining of R5 neurons and neurotransmitter-labeled cell bodies. R5 neurons are labeled with *R58H05-QF2-7>mtdTomato* (anti-dsRed, red). Neurotransmitter expression of

cell bodies is labeled either by anti-GABA (top row) antibody (anti-GABA, green) or MIMIC line insertions for ChAT (middle row, *ChAT^{MI}-GAL4>Stinger*) or vGluT (bottom row, *vGluT^{MI}-GAL4>Stinger*) driving Stinger (anti-GFP, green) expression. Arrows indicate R5 cell bodies which show co-labeling with neurotransmitter. Representative images are shown. Scale bar indicates 10 μm.

(C) Neuronal cell counts of R5 neurons and co-labeling with GABA, ChAT, and vGluT. In *R58H05-QF2-7>mtdTomato* animals stained with anti-GABA (n=6), an average of 6.8 out of 22.8 R5 neurons per brain were co-stained with GABA. For *R58H05-QF2-7>mtdTomato* animals with *ChAT^{MI}-GAL4>Stinger* (n=8), an average of 6.4 out of 20.4 R5 neurons per brain were cholinergic. No R5 neurons in *R58H05-QF2-7>mtdTomato*, *vGluT^{MI}-GAL4>Stinger* animals (n=8) were observed to have vGluT co-labeling. Mean ±SEM is shown. These data are quantified from imaging experiments in Figure 3B.

(D) Sleep profiles of *R58H05-GAL4>UAS-ChAT-miR* (blue), *R58H05GAL4>iso31* (gray), and *iso31>UAS-ChAT-mir* (black) flies. Sleep time plotted in 30 min bins. White and black bars indicate 12 hr light and dark periods, respectively. The period of sleep deprivation via mechanical shaking is indicated with a gray background. Data are from same flies as in (E) and (F).

(E and F) Baseline total sleep time (TST) (E) and rebound sleep from ZT0-6 (F) for *R58H05GAL4>iso31* (n=64), *iso31>UAS-ChAT-miR* (n=60), and *R58H05-GAL4>UAS-ChAT-miR* (n=60). Mean ± SEM is shown; one way ANOVA with Tukey's post hoc test.

(G) Sleep profiles of *R58H05-QF2-A>QUAS-dTRPA1; R19G02-GAL4>UAS-TNT* (magenta), *R19G02-GAL4>UAS-TNT* (gray), and *R58H05-QF2-A>QUAS-dTRPA1* (blue) flies. Sleep time plotted in 30 min bins. White and black bars indicate 12 hr light and dark periods, respectively. The period of dTRPA1 activation at 29°C from ZT12-24 is indicated with a yellow background. Data are from same flies as in (H) and (I).

(H and I) Sleep during (H) and after (I, ZT0-6) dTRPA1 activation for *R58H05-QF2-A>QUAS-dTRPA1* (n=48), *R58H05-QF2-A>QUAS-dTRPA1; R19G02-GAL4>UAS-TNT* (n=53), and *R19G02-GAL4>UAS-TNT* (n=56) flies. Mean ± SEM is shown; one way ANOVA with Tukey's post hoc test. See also Figure S3.

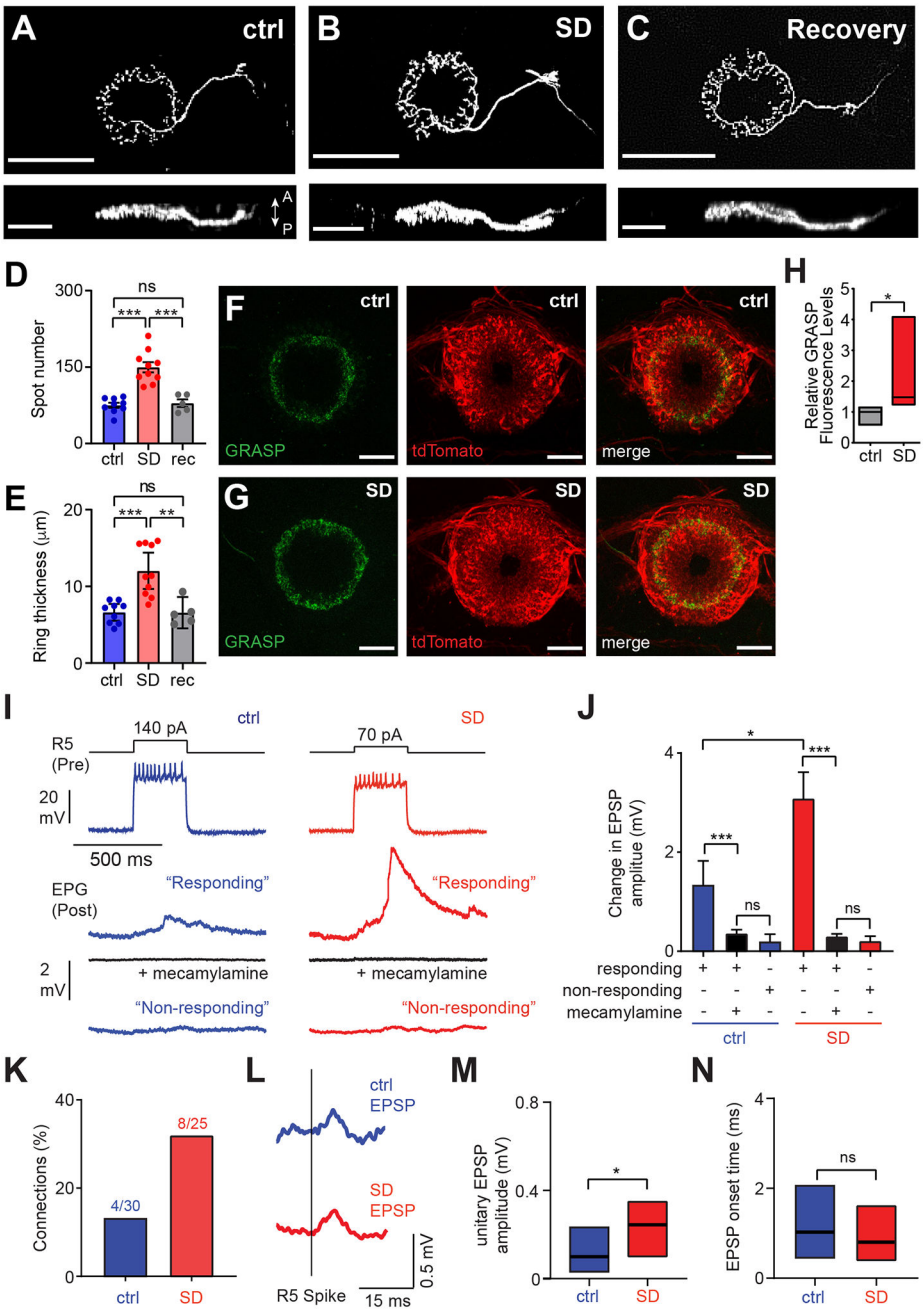

Figure 4. Functional Connectivity between R5 and EPG Neurons increases with Greater Sleep Need

(A–C) Representative single cell dye-fill images of R5 neurons in *R58H05-GAL4>UAS-CD4::tdGFP* animals after baseline sleep at ZT0-3 (A, ctrl), mechanical sleep deprivation at (SD) from ZT12-24 (B), or 12 hr recovery after SD (C). Upper and lower panels provide anterior/posterior and dorsal/ventral views, respectively. Scale bars denote 50 μm and 25 μm in upper and lower panels, respectively. Arrows indicate anterior (A) and posterior (P) directions.

(D and E) Number of spots in the ring region (D) and anterior-posterior ring thickness (E) of R5 neurons in control (blue, n=9), SD (red, n=10), and 12 hr recovery (gray, rec, n=5) animals, as described in (A–C); one-way ANOVA with post-hoc Tukey's test.

(F and G) Representative EB ring GRASP, tdTomato, and merged signals for R5 and EPG neurons in *R30G03-AD, R58H05-DBD>UAS-syb-spGFP1-10; R19G02-LexA>LexAop-CD4-spGFP11, LexAop-tdTomato* animals with (G) and without SD (F). Scale bar denotes 20 μm.

(H) Relative GRASP fluorescence levels (GFP/tdTomato) for the flies described in Figures (F) and (G) in the absence (gray, n=4) and presence of 12 hr SD (red, n=7); Mann-Whitney U test. Simplified box plots show 25^{th}, 50^{th}, and 75^{th} percentiles.

(I) Traces from paired recordings of R5 (presynaptic, Pre) and EPG (postsynaptic, Post) neurons from *R19G02-GAL4, R58H05-GAL4>UAS-CD4::tdGFP* flies in the absence (ctrl, blue) or presence (SD, red) of SD from ZT12-24. Activation of R5 neurons elicited small but detectable depolarization responses in paired EPG neurons at baseline, whereas concomitant SD triggered a greater response in paired EPG cells. Top: Representative R5 membrane voltage in response to a depolarizing current injection (140 pA and 70 pA for ctrl and SD conditions, respectively). Middle: Averaged traces of simultaneously recorded EPG membrane voltages from cells exhibiting a "response", without or with 50 μM mecamylamine (black). Bottom: Averaged traces of simultaneously recorded EPG membrane voltage showing "no response."

(J) Mean EPG membrane voltage change in the paired recordings described in (I), for "responding" cells in the presence and absence of mecamylamine and "non-responding" cells in animals at ZT0-3 following baseline sleep (ctrl, n=30) or 12 hr SD (SD, n=25); two-way ANOVA with post hoc Tukey's test.

(K) Frequency of synaptic connections identified between R5 and EPG pairs, in the presence (red) or absence (blue) of SD.

(L) R5 spike-triggered average of putative unitary EPG EPSPs in the presence (red) or absence (blue) of SD. Timing of R5 spikes is shown.

(M and N) Amplitude (M) and onset time (defined as a response reaching 10% of EPSP peak) (N) of R5 spike-triggered EPG EPSPs; Mann-Whitney U tests. Simplified box plots show 25^{th}, 50^{th}, and 75^{th} percentiles. Data shown in panels (I)-(N) are from the same flies. See also Figure S4.

KEY RESOURCES TABLE

REAGENT or RESOURCE	SOURCE	IDENTIFIER
Antibodies		
Rabbit polyclonal anti-GABA	Sigma	Cat# A2052 RRID: AB_477652
Mouse monoclonal anti-ChAT	Developmental Studies Hybridoma Bank	Cat# 4B1 RRID: AB_528122
Rabbit polyclonal anti-vGluT	Daniels et al.[33]	RRID: AB_2567386,
Chicken polyclonal anti-GFP	Invitrogen	Cat# A10262 RRID: AB_2534023
Rabbit polyclonal anti-dsRed	Clontech	Cat # 632496 RRID: AB_10013483
Mouse monoclonal anti-BRP	Developmental Studies Hybridoma Bank	Cat# nc82 RRID: AB_2314866
Alexa Fluor 488 Goat anti-Chicken IgY	Invitrogen	Cat# A11039 RRID: AB_2534096
Alexa Fluor 568 Goat anti-Mouse IgG	Invitrogen	Cat# A11031 RRID: AB_144696
Alexa Fluor 647 Goat anti-Mouse IgG	Invitrogen	Cat# A21235 RRID: AB_2535804
Alexa Fluor 568 Goat anti-Rabbit IgG	Invitrogen	Cat# A11011 RRID: AB_143157
Rabbit polyclonal anti-GFP	Thermo Fisher	Cat# A11122 RRID: AB_221569
Alexa Fluor 488 Goat anti-Rabbit IgG	Thermo Fisher	Cat# A27034 RRID: AB_2536097
Alexa Fluor 568-conjugated streptavidin	Thermo Fisher	Cat# S11226
Bacterial and virus strains		
N/A		
Biological samples		
N/A		
Chemicals, peptides, and recombinant proteins		
Collagenase	Sigma	Cat# C5138
Protease XIV	Sigma	Cat# P5147
Dispase	Sigma	Cat# D4693
Escin	Santa Cruz Biotechnology	Cat# 6805-41-0
Mecamylamine	Sigma	Cat# M9020

REAGENT or RESOURCE	SOURCE	IDENTIFIER
Critical commercial assays		
N/A		
Deposited data		
N/A		
Experimental models: Cell lines		
N/A		
Experimental models: Organisms/strains		
iso31	Bloomington *Drosophila* Stock Center	BDSC# 5905
R19G02-GAL4	Bloomington *Drosophila* Stock Center	BDSC# 48860
SS50574 (VT017491-AD, VT043927-DBD)	Janelia	SS50574
R60D05-GAL4	Bloomington *Drosophila* Stock Center	BDSC# 39247
R15C03-GAL4	Bloomington *Drosophila* Stock Center	BDSC# 47865
R58H05-GAL4	Bloomington *Drosophila* Stock Center	BDSC# 39198
R46C03-GAL4	Bloomington *Drosophila* Stock Center	BDSC# 50258
R30G03-GAL4	Bloomington *Drosophila* Stock Center	BDSC# 49646
R69F08-GAL4	Bloomington *Drosophila* Stock Center	BDSC# 39499
R58H05-QF2 #7	Blum et al.[2]	
R58H05-QF2 #A	Wu Lab	
R58H05-AD (86Fb), R46C03-DBD (vk27)	Blum et al.[2]	
R30G03-AD (86Fb), R58H05-DBD (vk27)	Liu et al.[1]	
R19G02-LexA	Bloomington *Drosophila* Stock Center	BDSC# 52550
UAS-ChAT-miR1-A	Wu Lab	
UAS-mCD8-GFP	Bloomington *Drosophila* Stock Center	BDSC# 5137
UAS-dTRPA1	Bloomington *Drosophila* Stock Center	BDSC# 26263
UAS-TNT	Bloomington *Drosophila* Stock Center	BDSC# 28838
UAS-CD4-tdGFP	Bloomington *Drosophila* Stock Center	BDSC# 35836
UAS-mtdTomato	Bloomington *Drosophila* Stock Center	BDSC# 30124
$ChaT^{MI04508}$-GAL4	Bloomington *Drosophila* Stock Center Diao et al.[17]	BDSC# 60317
$vGluT^{MI04979}$-GAL4	Bloomington *Drosophila* Stock Center. Diao et al.[17]	BDSC# 60312
UAS-Stinger	Bloomington *Drosophila* Stock Center	BDSC# 84277

Curr Biol. Author manuscript; available in PMC 2023 November 21.

REAGENT or RESOURCE	SOURCE	IDENTIFIER
QUAS-dTRPA1-7	Gift of C. Potter	
UAS-spGFP1-10	Bloomington *Drosophila* Stock Center	BDSC# 93016
lexAop-CD4-spGFP11	Bloomington *Drosophila* Stock Center	BDSC# 93019
LexAop-tdTomato	Bloomington *Drosophila* Stock Center	BDSC# 77138
UAS-syt-GFP, UAS-DenMark	Bloomington *Drosophila* Stock Center	BDSC# 33065
10XUAS-syn21-GFP-p10 (attP2) pJFRC81	Gift of G. Rubin	Pfeiffer et al.[34]
20XUAS-IVS-dTRPA1 (attP18) pJFRC124	Gift of G. Rubin	
ppk-Gal80	Gift of W. Joiner	
MB247-GAL4	Bloomington *Drosophila* Stock Center	BDSC# 50742
20XUAS-6XGFP	Bloomington *Drosophila* Stock Center	BDSC# 52261
10XQUAS-6XGFP	Gift of C. Potter	
Oligonucleotides		
Oligo 5’ ATAGAATTCCGCCAGATCTTTTAAAGTCCACAACTCATCAAGGAAAAT GAAAGTCAAAGTTGGCAGCTTACTTAAACTTAATCACAGCCTTTAAT GTACCGCTGGCTGGGAACTTTCATTAAGTTAATATACCATATCTAATTAAAGT TCCCAGCCAGCGGTGTACCTAAAGTGCCTAACATCATTATTTAATTTTTTTTTTTTT TGGCACACGAATAACCATGCCGTTTTGGATCTTTTAAAGTCCACAACTCATCAAGGAAAATGAAAGTCAAAGTTGGCAGCTTAC TTAAACTTAATCACAGCCTTTAATGTAGATGCACGAGCTGTTCAAC GATAAGTTAATATACCATATCTATCTTTGAACAGCTCGTGCATCTGTACCTAAA GTGCCTAACATCATTATTTAATTTTTTTTTTTTTTGGCACACGAATAACCATGCCGTTTTGGATCCGTGCGGCCGCAAC 3’	GeneArt	*UAS-ChaT-miR*
Recombinant DNA		
pUAST	Brand and Perrimon[35]	
Software and algorithms		
FIJI	Open Source	https://imagej.net/software/fiji/ RRID: SCR_002285
MATLAB	Mathworks	RRID: SCR_001622
Custom MATLAB Scripts for sleep analysis	Blum et al.[2]	https://github.com/marknwulab/Blum-et-al.-2020
Custom Python code in Jupyter Notebook	Wu Lab	https://github.com/margiezilla/Ho_etal_2022
Prism 7	Graphpad	RRID: SCR_002798
DAMFileScan311	Trikinetics	N/A
DAMFileScan113	Trikinetics	N/A
Zen Black	Zeiss	RRID:SCR_013672
Jupyter Notebook	https://jupyter.org/	RRID:SCR_018315
Python Programming Language	http://www.python.org/	RRID:SCR_008394
Other		

REAGENT or RESOURCE	SOURCE	IDENTIFIER
Dental Wax	GC Corp	Cat# 27B2X00008000016
DAM2 Activity Monitors	Trikinetics	Cat# DAM2
LC-4 Light Controller	Trikinetics	Cat# LC4
PSIU9 Power Supply Interface	Trikinetics	Cat# PSIU9
Vortexer with Vortex Mounting Plate	Trikinetics	Cat# TVOR-120
Laser-cut Adaptor Plate for Vortexer	Wu Lab	https://github.com/marknwulab/Blum-et-al.-2020
DVX-2500 Digital Multi-tube Vortexer	VWR	DVX-2500